Nanoscale

RSC Publishing

PAPER

View Article Online
View Journal | View Issue

Cite this: *Nanoscale*, 2013, **5**, 8029

A general single-pot heating method for morphology, size and luminescence-controllable synthesis of colloidal ZnO nanocrystals†

Xin Liu and Mark T. Swihart*

Received 18th May 2013
Accepted 5th July 2013

DOI: 10.1039/c3nr02571c

www.rsc.org/nanoscale

Here we demonstrate a single-pot heating approach for controllable synthesis of colloidal zinc oxide nanocrystals from zinc acetylacetonate. Such single-pot heating approaches are inherently amenable to large scale production. We have systematically studied the crystallization process, investigating the growth of nanocrystals and the influence of ligands on the morphology and luminescence of ZnO nanoparticles. We show that the morphology can be tuned to produce dendritic structures, nano-needles, nano-pinecones, nanoclusters, hexagonal pyramid nanoparticles and irregularly-shaped nanoparticles by varying the surfactants and co-surfactants used in synthesis. Moreover, we investigated the effect of ligands on the defect-related photoluminescence of ZnO NPs and demonstrated blue, green, white, yellow, and orange emission. This study opens up new possibilities for the practical use of ZnO nanomaterials for optoelectronic devices and bio-imaging.

Introduction

Semiconductor nanocrystals have attracted much interest over the past two decades, due to their distinct and useful physical properties.[1–4] They have many potential applications, ranging from biological labeling[5,6] to photovoltaic devices.[7–10] Zinc oxide is a semiconductor with a wide band gap (3.37 eV)[11,12] and large exciton binding energy of 60 meV.[13] Doped ZnO can exhibit efficient photoluminescence at various visible wavelengths,[14] and heavily-doped ZnO can exhibit plasmon resonance.[15–17] ZnO is of interest for diverse electronic and optical applications including solar cells,[18–20] piezoelectric generators,[21] field-effect transistors,[22] and UV lasers.[23] Moreover, ZnO is relatively biocompatible and therefore amenable to use in bioimaging[24,25] and related applications.

Both size and shape are key factors influencing the properties of semiconductor nanocrystals. Therefore, control of morphology and size during synthesis is of great interest. A valuable general approach to synthesizing semiconductor nanocrystals is thermolysis of precursors in high-boiling-point organic solutions.[1,26] In this approach, several factors play important roles in determining nanocrystal morphology and size.[27,28] These include concentration of monomers,[29] precursor structure,[30] identity of ligands,[31–33] temperature,[34,35] and reaction modality (*e.g.* hot-injection *vs.* a single-pot heating approach). The size distribution of semiconductor nanocrystals particularly sensitive to the concentration of monomer in the solution from which they are synthesized.[36] Typically, an initial high concentration generates a burst of nucleation.[37] If this is followed by growth at lower concentration[29] where further nucleation does not occur, then narrowing or "focusing" of the size distribution is possible.[26,38] Depletion of monomer during the growth stage can induce Ostwald ripening which broadens the size distribution.[39] Ligands play a critical role through interactions with both monomers and particles during the process of forming nanocrystals.[31] For example, Peng *et al.*[31] synthesized both isotropic and anisotropic CdTe nanocrystals by employing different surfactants and their combinations. The bonding strength of such ligands to monomers can significantly influence the activity of monomers in solution, providing an effective concentration (*i.e.* activity) lower than the actual concentration. When the activity of monomer is high enough, anisotropic shapes such as nanorods, tetrapods and dendritic structures may form. These are generally non-equilibrium structures whose shape is governed by the kinetics of growth on different crystal facets. By combining ligands in a one-pot reaction, the distinct selectivity and varied bonding strength of ligands to different crystal planes can be used to control the growth kinetics and form anisotropic nanostructures.

In materials with two crystalline polymorphs of comparable stability, crystal phase plays a central role in controlling the growth of anisotropic structures. For example, the landmark work of Manna *et al.*[40] clearly showed that CdSe tetrapods grow with a zincblende core and wurtzite arms, and that both wurtzite and zincblende can co-exist in CdSe nanorods. Some other anisotropic CdSe structures (arrows, *etc.*) were predominantly wurtzite. For ZnO, the cubic polymorph is significantly less

Department of Chemical and Biological Engineering, University at Buffalo (SUNY), Buffalo, NY 14260, USA. E-mail: swihart@buffalo.edu

† Electronic supplementary information (ESI) available. See DOI: 10.1039/c3nr02571c

stable than the hexagonal polymorph (wurtzite or zincite structure). We did not see any evidence of cubic ZnO in this study, and therefore believe that phase behaviour is not an important factor controlling shape evolution in this particular system.

Recently, various methods have been explored for obtaining nanoscale ZnO with diverse morphologies including hexagonal pyramids,[41] nanobelts,[42] nanowires,[23,43] nanotubes,[44,45] nanorings,[46] and nanorods.[47,48] Physical methods,[46,49] especially growth of anisotropic ZnO on different substrates, are widely used for preparing one-dimensional nanostructures such as nanowires and nanotubes. For obtaining substrate-free nanocrystals, however, chemical solution methods involving thermolysis of zinc precursors in the presence of surfactants are used. Zinc acetate[50] and zinc stearate[28] have been widely used in ZnO nanocrystal synthesis. These precursors interact with organic surfactants such as oleylamine to form Zn–ligand complexes that can be thermally decomposed to generate ZnO nanoparticles. Metal ions chelated with acetylacetonate ligands are extensively employed as precursors for synthesizing magnetic nanoparticles[51–53] of materials including iron oxide,[53] core–shell iron@iron oxide,[54] cobalt,[55] nickel and nickel oxide,[52] and MFe_2O_4 (M = Co, Mn).[51] In particular, synthesis of iron oxide and other ferrite nanoparticles from acetylacetonate precursors can produce very uniform nanoparticles using single-pot heating protocols. Based on this success, zinc acetylacetonate ($Zn(acac)_2$) is also a precursor of interest for ZnO nanocrystal synthesis.[51,53]

In this report, we demonstrate a general single-pot heating protocol to synthesize ZnO nanoparticles from $Zn(acac)_2$. We demonstrate the preparation of particles of controlled size and shape, in most cases without relying on rapid hot injection and mixing. With zinc acetylacetonate as precursor, we systematically studied different combinations of organic ligands impacting the morphology, size and photoluminescence spectra of ZnO nanocrystals. In contrast to the popular hot-injection method of preparing nanocrystals, this direct single-pot heating method is simpler and much more amenable to scale up. While hot-injection approaches are quite sensitive to the details of mixing during and following injection, the one-pot heating up approach is less sensitive to details of mixing, and simply requires sufficient mixing to maintain a uniform temperature, which is achievable even at very large scale.

Experimental section

Chemical reagents

Zinc(II) acetylacetonate ($Zn(acac)_2$, Sigma Aldrich), oleylamine (80–90%, Fisher Scientific), trioctylphosphine oxide (TOPO, technical grade 90%, Sigma Aldrich), oleic acid (technical grade 90%, Fisher Scientific), trioctylamine (98%, Sigma Aldrich), octylamine (99%, Sigma Aldrich), benzyl ether (99%, Sigma Aldrich), phenyl ether (99%, Sigma Aldrich), 1,2-hexadecanediol (technical grade, 90%, Sigma Aldrich), dodecanethiol (≥98%, Sigma Aldrich), octanethiol (≥98.5%, Sigma Aldrich), and octadecanol (99%, Sigma Aldrich) were used as received.

Synthesis of dentritic branched ZnO nanostructures

300 mg $Zn(acac)_2$ was mixed with 7 mL benzyl ether, 2.2 g TOPO and 735 mg hexadecanediol in a 100 mL three-neck flask and heated. The solution was heated to 285 °C or 300 °C at a rate of 15 °C min^{-1} and held at constant temperature for 70 minutes to produce branched ZnO nanostructures. Nanocrystals prepared at higher temperature showed improved crystallinity. Crystal splitting was observed during synthesis and the shape evolution was studied by stopping the reaction at different time points. Fan-like ZnO nanostructures were synthesized by quickly injecting the premixed 735 mg hexadecanediol and 2 mL benzyl ether into 263 mg $Zn(acac)_2$ dissolved in 1.93 g TOPO at 290 °C and maintaining this temperature for 70 min. Other reaction conditions were the same as those used to synthesize branched ZnO nanostructures.

Synthesis of hexagonal pyramid ZnO nanoparticles

150 mg $Zn(acac)_2$, 1.13 mL oleylamine, 0.54 mL oleic acid, 10 mL phenyl ether and 1.47 g hexadecanediol were mixed together. The solution was heated to 260 °C a rate of 15 °C min^{-1}. The solution was kept at 260 °C for 25 min.

Synthesis of cluster-like ZnO nanocrystals

150 mg $Zn(acac)_2$ was dissolved directly in 7 mL oleylamine and 1.08 mL oleic acid at 120 °C and the solution was stirred for 1 h. After adding 367 mg hexadecanediol, the solution was rapidly heated to 300 °C. Upon removal of the heating mantle, the temperature dropped to 265 °C where it was held for 3.5 min.

Synthesis of needle-like and pinecone-like ZnO nanostructures

300 mg $Zn(acac)_2$, 3.5 mL trioctylamine, 0.72 mL oleic acid and 367 mg hexadecanediol were loaded in a three-neck flask at room temperature. Then the solution was heated to 298 °C at a rate of 20 °C min^{-1}. The system was maintained at this temperature for 70 min then cooled gradually to 50 °C. Needle-like ZnO nanostructures were then precipitated by adding ethanol or methanol followed by centrifugation and re-dispersion in chloroform or hexane. Cone-like ZnO nanostructures were obtained upon increasing the scale of this synthesis by a factor of three (900 mg $Zn(acac)_2$ 10.5 mL trioctylamine, 2.16 mL oleic acid and 1.10 g hexadecanediol) while otherwise using the same nominal reaction conditions and procedures.

Synthesis of 9–10 nm ZnO nanoparticles

200 mg $Zn(acac)_2$ was mixed with 7 mL benzyl ether, 2.2 g TOPO and 763 mg octadecanol. Upon heating to about 120 °C, this mixture became transparent. It was then rapidly heated to 295 °C. The solution was held at this temperature for 40 min then allowed to cool gradually to 50 °C.

Synthesis of 2–3 nm ZnS nanoparticles

150 mg $Zn(acac)_2$ was mixed with 7 mL benzyl ether in the presence of 0.95 mL dodecanethiol and 367 mg

1,2-hexadecanediol. The mixture was then heated rapidly to 260 °C at a rate of 20 °C min^{-1} and held at that temperature for 50 min.

Separation and purification of ZnO NPs

ZnO NPs were collected by adding ethanol to destabilize the dispersion, then centrifuging at approximately 8000 × *g*. As-collected ZnO NPs were redispersed in hexane or chloroform. Ethanol was added to the solution and ZnO NPs were again collected by centrifugation. The procedure was repeated twice in order to adequately remove unreacted precursor and surfactants.

Characterization

Transmission electron microscopy (TEM). The morphology and size of ZnO nanocrystals were determined by transmission electron microscopy (TEM) using a JEOL JEM-2010 microscope at a working voltage of 200 kV. Samples were prepared for imaging by dropping the dilute ZnO NP dispersion onto a carbon-coated copper TEM grid (Ted Pella, 1822-F) and allowing excess solvent to evaporate.

Selected area electron diffraction (SAED). SAED patterns were obtained in the same JEM-2010 microscope.

X-ray diffraction (XRD). The crystal structure of ZnO nanocyrstals was determined using X-ray diffraction (XRD, Bruker Ultima IV with Cu Kα X-ray source). The samples were prepared by drop-casting highly-concentrated colloidal ZnO nanocrystal dispersions on glass substrates and evaporating the solvent.

UV-vis-NIR spectroscopy. Optical absorption of ZnO nanoparticles was measured using a Shimadzu 3600 UV-visible-NIR scanning spectrophotometer.

Photoluminescence spectroscopy. Photoluminescence (PL) spectra were measured using a Fluorolog-3 spectrofluorometer (Jobin Yvon). The excitation wavelength was set to 365 nm and the emission was scanned from 400 nm to 800 nm.

Results and discussion

Dendritic branched and fan-like ZnO nanostructures

TEM images of dendritic, branched ZnO nanostructures synthesized by thermolysis of 300 mg $Zn(acac)_2$ in the presence of 2.2 g TOPO, 7 mL benzyl ether and 735 mg hexadecanediol at 285 °C and 300 °C, are shown in Fig. 1. Upon reducing the concentration of zinc precursor to 150 mg, under otherwise identical conditions, no such branched nanostructures were observed. Instead ZnO nanoparticles were formed in high yield. Selected-area electron diffraction (SAED) showed that the ZnO nanoparticles produced at lower $Zn(acac)_2$ concentration were amorphous or semi-crystalline (Fig. S1†).

Moreover, amorphous ZnO NPs were generated whenever the reaction temperature was less than 250 °C. The crystallization process is impacted by both thermodynamic and kinetic factors, two of which are concentration and temperature. From a thermodynamic perspective, there exists a critical radius above which a particle nucleus is stable, determined by the Gibbs energy change for going from precursor to solid and by the surface energy of the solid (as modified by any surfactant adsorbed to that surface). The critical radius decreases with both increasing concentration of monomer and increasing temperature. Our observation that there exists a minimum activation temperature and critical precursor concentration to trigger the reaction is consistent with this basic theory of nucleation. We investigated the time-dependent growth of dendritic branched ZnO nanostructures by quenching the reaction at different time points. Fig. 2A shows the time-dependent morphological evolution of ZnO nanostructures

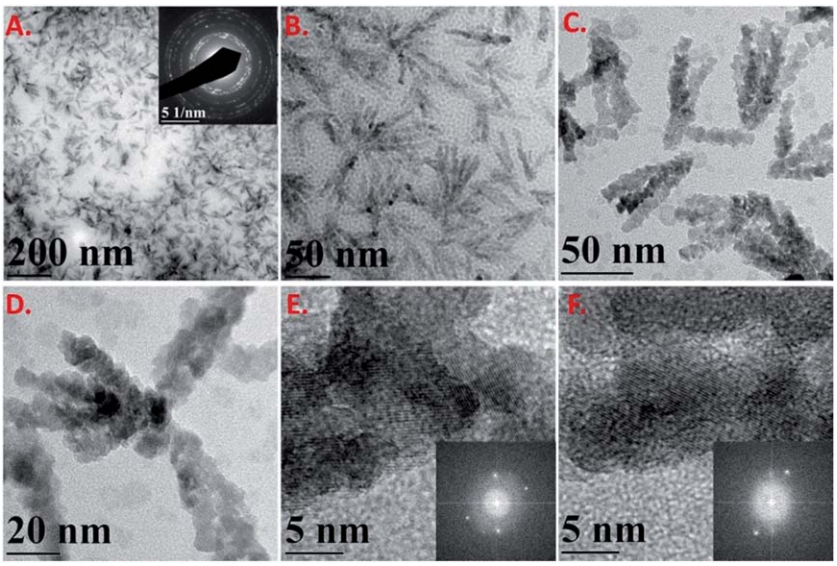

Fig. 1 (A and B) TEM images showing the morphology of dendritic branch-like ZnO nanostructures prepared at 285 °C. The inset in (A) shows a selected area electron diffraction (SAED) pattern demonstrating the crystallinity of the nanostructures. (C and D) TEM and (E and F) HRTEM images showing the morphology of branch-like ZnO nanostructures synthesized at 300 °C. The (1,0,1) crystal planes are clearly visible in the HRTEM images. Insets in (E) and (F) are the fast Fourier transforms (FFTs) of the images.

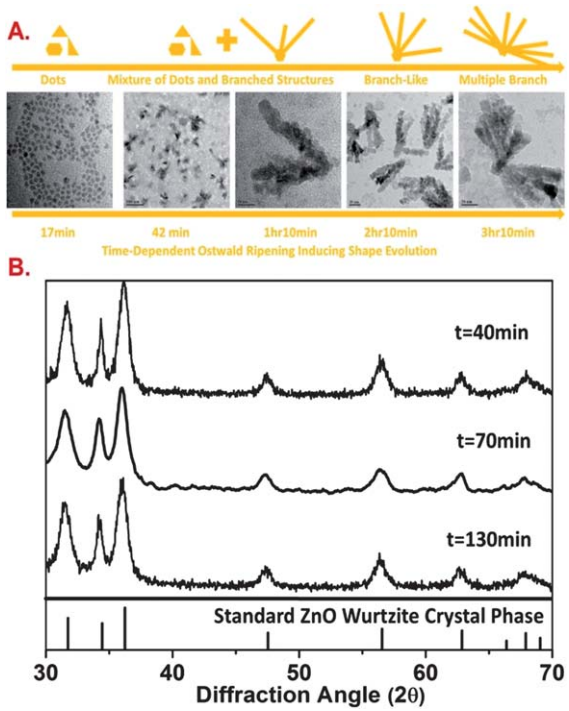

Fig. 2 (A) Shape evolution induced by crystal splitting, illustrated through TEM images at increasing reaction times. (B) XRD patterns of branched ZnO nanocrystals at different reaction times.

synthesized at 300 °C. ZnO NPs show poor crystallinity at reaction times less than 17 min. These amorphous particles appear to be a metastable precursor from which the crystalline dendritic particles form. After 40 min, a few crystalline dendritic particles mixed with a large amount of amorphous particles are observed. With increasing aging time, the amorphous particles gradually disappear and the crystalline dendritic particles grow. This phenomenon is similar to the synthesis of Bi_2S_3 sheaf nanostructures reported by Alivisatos' group.[56] As in that work, the formation of anisotropic ZnO nanostructures could be attributed to crystal splitting at high crystal growth rates. This occurs at monomer concentrations and temperature above some critical value that varies from material to material.[56] Moreover, further splitting of dendritic ZnO nanostructures was observed with increased reaction time.[54] High-resolution TEM (HRTEM) showed the (1,0,1) crystal planes in the ZnO nanocrystals. XRD showed that the nanobranched ZnO grew as the bulk ZnO wurtzite phase. No obvious changes in the XRD pattern were observed with increasing reaction time.

Interestingly, we found that fan-like ZnO nanostructures were formed if we injected 1,2-hexadecanediol into hot Zn(acac)$_2$/TOPO solution at 290 °C instead of heating the premixed Zn(acac)$_2$, TOPO, and 1,2-hexadecanediol. The mixture was then held at 290 °C for 70 minutes to produce the fan-like structures shown in Fig. 3. We speculate that, hexadecanediol serves to increase the crystal growth rate. Thus, its sudden addition could lead to a burst of multiple crystal splitting events, that would produce this fan-like morphology. However, further work would be required to establish whether this proposed mechanism is operative here.

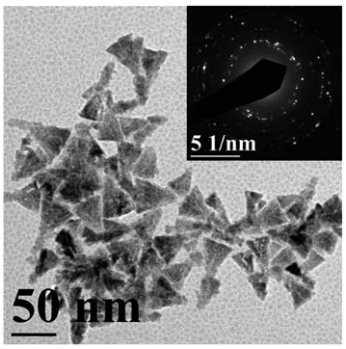

Fig. 3 TEM image of ZnO nanocrystals with fan-like morphology. The inset is the selected-area electron diffraction (SAED) pattern.

6–10 nm ZnO nanocrystals with pyramidal morphology

ZnO nanocrystals with pyramidal morphology were synthesized by thermolysis of 150 mg Zn(acac)$_2$ in the presence of 1.13 mL oleylamine, 0.54 mL oleic acid, 10 mL phenyl ether and 1.47 g hexadecanediol at 260 °C. HRTEM (Fig. 4B) revealed triangular and hexagonal projections, corresponding to hexagonal pyramid ZnO NPs lying on their side or standing up, respectively. Fig. 4C shows the hexagonal morphology that was attributed to such ZnO NPs standing on their bases. Moreover, HRTEM images indicated that the growth of pyramid was along [0,0,2] direction corresponding to the *c*-axis of ZnO wurtzite crystal structure.

Preparation of nonequilibrium nanostructures in pure coordinating solvents: cluster-like nanoparticles, needle-like nanoparticles and nano-pinecone structures

During nucleation, formation of a high concentration of nuclei can induce fast depletion of monomers. A result of this can be that the solution phase monomer concentration is too low to drive anisotropic growth. Anisotropic particles have higher

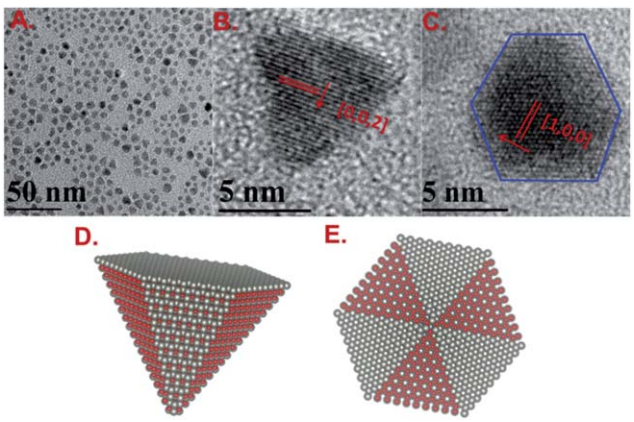

Fig. 4 (A) TEM image of ZnO hexagonal pyramids 6–10 nm in diameter. (B) HRTEM image showing the triangular morphology corresponding to NPs lying on their side and (C) hexagonal shapes attributed to NPs standing up. Panels (D) and (E) show a side-view and top-view, respectively of a ball-and-stick model of a wurtzite ZnO hexagonal pyramid nanocrystal. The base of the pyramid is a [0,0,2] plane. Zn atoms are grey, O atoms are red.

chemical potential than spheres or quasi-spherical faceted shapes. Thus, kinetically-driven anisotropic growth requires a higher monomer activity (effective concentration) than growth of isotropic structures. Thus, anisotropic growth can be favoured by high monomer concentration and a low nucleation rate that does not deplete the monomers in solution. The monomer activity,[31] which represents the effective concentration, is typically lower than the actual concentration, because the monomers are complexed with other species in solution. Thus, in addition to the actual precursor concentration, the monomer activity in solution is influenced by both the identity and concentration of ligands.

We investigated synthesis of ZnO NPs in pure coordinating solvents (*i.e.* ligands). ZnO NPs with non-equilibrium cluster-like morphology were obtained if the reaction was carried out in mixtures of oleylamine (OAm) and oleic acid (OA), without phenyl ether (Fig. 5A and B). The activity of the monomers decreased with increasing concentration of OAm and OA due to the strong coordination of zinc ions by these species. Lower monomer activity (at the same actual monomer concentration) results in lower nucleation rate during in the nucleation stage. This increased the amount of precursor remaining in solution after the initial nucleation burst, which favored anisotropic growth. We also observed that ZnO NPs with regular hexagonal shape (Fig. 5C) were formed if the quantity of Zn precursor was doubled. We suggest that the higher Zn monomer activity in this case promoted rapid depletion of monomers to a larger number of nuclei, which left insufficient monomer concentration in solution to promote anisotropic growth of ZnO NPs. Instead, Ostwald ripening occurred during the growth stage, resulting in a broad size distribution of ZnO NPs.

We also tested the combination of trioctylamine (TOA) and oleic acid (OA) as ligands. ZnO NPs with non-equilibrium needle-like structure were produced in this case. TEM images (Fig. 6A and B) revealed the diameter and average length of as-prepared ZnO nanoneedles were 1–2 nm and 35 nm, respectively. Interestingly, ZnO NPs with a pinecone shape (Fig. 6C and D) were produced when the scale of the reaction was increased. HRTEM (Fig. S2†) revealed the pine-cone NPs were composed of small ZnO nanocrystals. A similar phenomenon has been reported in the synthesis of CdTe tetrapods and nanorods when the reaction scale was amplified, although the origin of this effect is not entirely clear.[55] This result was unexpected, in light of the expected scalability of the single-pot heating approach. We attribute the change in morphology to a difference in temperature distribution in the solution when the solution volume was tripled without changing other reaction parameters such as the flask size, heater power, stirring speed, or other conditions. This provides a cautionary note that even though, in principle, simple heating processes should be scalable, these nanocrystal synthesis processes can be very sensitive to the spatial and temporal distribution of temperature, which must therefore be carefully controlled during scale-up. Nonetheless, reproducing the same temperature and concentration profiles in a heating process like that used here will remain much easier than in a hot injection process, where the effects of changes in reaction scale are even more pronounced.

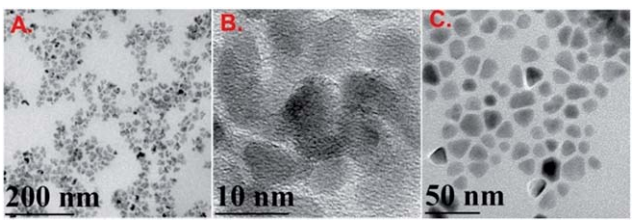

Fig. 5 (A) TEM and (B) HRTEM images of ZnO NPs synthesized in pure OA and OAm. (C) TEM image showing hexagonal ZnO NPs formed when the $Zn(acac)_2$ concentration was doubled.

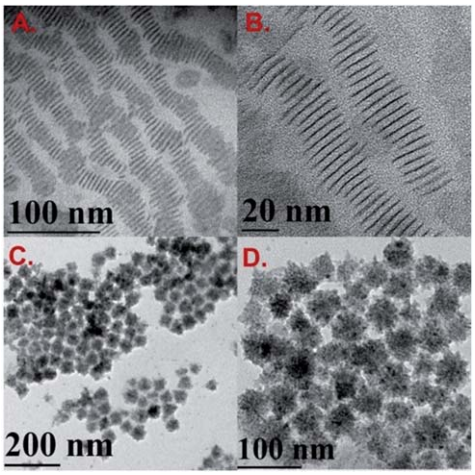

Fig. 6 TEM images of (A and B) needle-like ZnO nanostructures and (C and D) porous pinecone-like nanoparticles.

Monodisperse 9–10 nm ZnO nanocrystals

Alcohols and diols are used to accelerate decomposition of the metal acetylacetonate precursor to form metal oxide NPs. 1,2-Hexadecanediol has been most widely used to synthesize monodisperse magenetic oxide NPs, and was used in most of the experiments reported here. In one set of experiments, we replaced 1,2-hexadecanediol with octadecanol, which is lower in cost and more widely available than 1,2-hexadecanediol. However, octadecanol may be less effective in promoting precursor decomposition, because it has only one hydroxyl group. Monodisperse 9–10 nm ZnO nanocrystals with irregular shape (Fig. 7A and B) were obtained by thermolysis of 200 mg $Zn(acac)_2$ in the presence of 2.2 g TOPO, 7 mL benzyl ether and 736 mg octadecanol at 290 °C. The relatively low precursor concentration, along with use of octadecanol, reduced monomer activity, producing a lower growth rate, and resulting in formation of nanoparticles. However, branched ZnO nanostructures were formed if the $Zn(acac)_2$ quantity was increased to 300 mg (Fig. S3†). In that case, the higher monomer activity increased the growth rate and drove formation of anisotropic ZnO nanostructures, as also observed using 1,2-hexadecandiol.

Investigation of the effect of using alkyl-thiol ligands

Alkyl-thiols are widely used as capping agents for stabilizing NPs, and thus it was logical to explore their use in ZnO NP

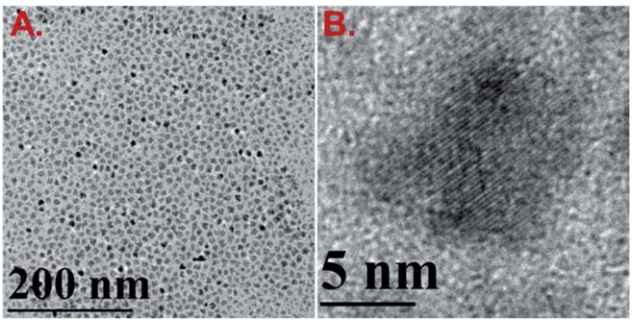

Fig. 7 (A) TEM and (B) HRTEM images of 9–10 nm ZnO NPs.

synthesis under the conditions used here. However, in the present case, ZnS NPs, rather than ZnO NPs, were produced when dodecanethiol or octanethiol was used as a ligand. This is consistent with a previous report of the use of an alkyl-thiols as sulfur donors for synthesis of semiconductor NCs.[57,58] Fig. 8A and B show the monodisperse ultrasmall ZnS NPs (2–3 nm) synthesized by heating $Zn(acac)_2$ in the presence of dodecanethiol. Powder XRD (Fig. 8C) confirmed that the NPs consisted of ZnS.

Photoluminesence of ZnO nanocrystals

Semiconductor nanocrystals are well known for their size-dependent optical properties. However, for ZnO, size-dependent photoluminescence cannot be observed at visible wavelengths because of its large intrinsic band gap (3.37 eV, in the ultraviolet). Thus, visible luminescence from ZnO is attributed to oxygen vacancies or other defects. In nanocrystals, surface defect emission plays a particularly important role, simply because of the high surface area of the material. If the defect-related emission is both efficient and controllable, then ZnO nanocrystals with visible luminescence could be competitive with other light-emitting inorganic nanostructures. ZnO nanocrystals with green, yellow and orange photoluminescence were reported recently. These can be synthesized using polymer templates during synthesis.[24]

The methods presented here provide a facile method to tune the luminescence of ZnO nanocrystals to produce different emission colors, including blue, green and yellow by simply using different ligands during synthesis. No prominent absorbance change around 350–360 nm was observed for products prepared with different surfactants (Fig. 9). Upon excitation of the ZnO nanocrystals at 365 nm, photoluminescence was observed, with a peak wavelength that depended upon the ligands used during synthesis (Fig. 10).

In pure coordinating solvents *i.e.* in the presence of oleylamine and oleic acid, the ZnO nanocrystals exhibit green luminescence with a peak emission wavelength of 495 nm. Similar blue luminescence with a peak at 445 nm can be observed for ZnO NPs synthesized using trioctylamine and oleic acid. For ZnO nanoparticles prepared using oleylamine as surfactant and benzyl ether as solvent, double emission peaks appeared at 590 nm and 635 nm. With increasing reaction time, the intensity of emission near 635 nm increased, changing the emission color from yellow to orange. This suggests that new

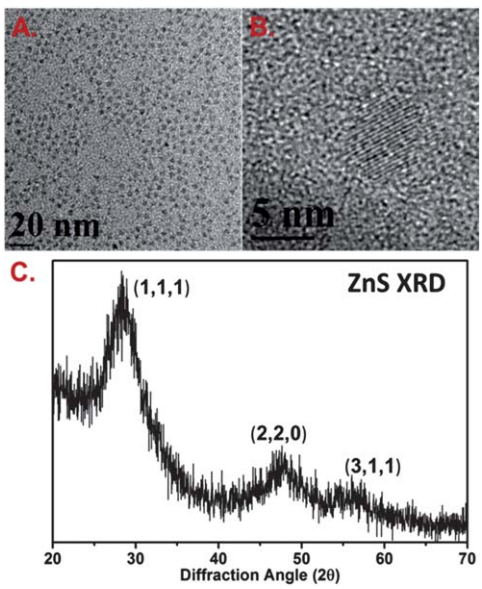

Fig. 8 (A) TEM and (B) HRTEM show monodisperse 2–3 nm ZnS NPs synthesized by using dodecanethiol as the capping ligand. (C) The XRD pattern of these NPs shows that they are ZnS and not ZnO.

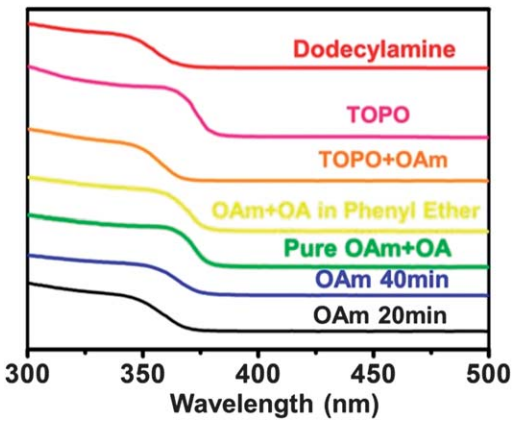

Fig. 9 Optical absorption of ZnO NPs synthesized using different ligands.

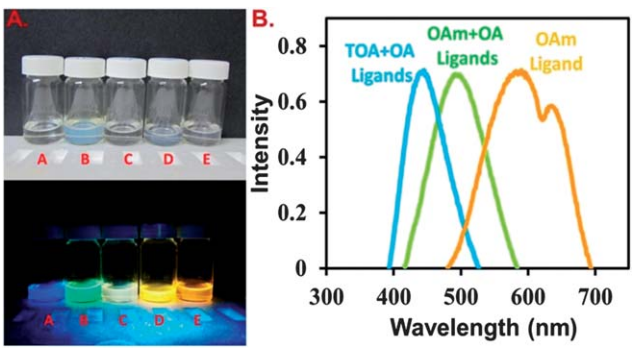

Fig. 10 Images and normalized photoluminescence spectra of ZnO nanocrystals synthesized in the presence of different capping ligands.

Table 1 Summary of the morphologies, sizes and luminescence colors of ZnO NCs synthesized under various conditions

$Zn(acac)_2$ (mg)	Surfactants	Benzy ether (mL)	Hexadecanediol (mg)	T (°C)	Time (min)	Morphology	Size (nm)	PL color
300	TOPO 2.2 g	7	735	285–300	70–200	Branch	N/A	N/A
150	OAm 2.63 mL	7	367	250	40	Particle	5–9	Orange
150	OAm 1.13 mL + OA 0.54 mL	Phenyl ether 10 mL	1470	260	25	Hexagonal pyramid	6–10	N/A
150	OAm 7 mL + OA 1.08 mL	N/A	367	290	20	Cluster-like	20–25	N/A
300	OAm 7 mL + OA 1.08 mL	N/A	367	280	20	Particle	15–25	Green
300	TOA 3.5 mL + OA 0.72 mL	N/A	367	300	70	Needle-like	(D) 1–2 (L) 35–50	Blue
900	TOA 10.5 mL + OA 2.16 mL	N/A	1101	300	70	Cone-like	45–50	N/A
150	DDT 0.95 mL	7	367	260	55	ZnS QDs	2–3	Blue
200	TOPO 2.2 g	7	Octadecanol 776	300	40	Particle	9–10	N/A
300	TOPO 2.2 g	7	Octadecanol 776	300	80	Branch	N/A	N/A
150	Dodecylamine 738 mg	7	367	295	60	Particle	4–6 nm	Yellow
150	TOPO 1.55 g + OAm 2.5 mL	N/A	735	205	30	Particle	5–6 nm	Yellow

defect states are introduced in this case, at energies deeper within the band gap. When the reaction time reached 70 min, the ZnO photoluminescence appeared white (Fig. 10, sample C), with the emission from the ZnO NPs spanning the visible spectrum. Addition of oleic acid to the synthesis, while keeping other reaction conditions constant, caused a blue-shift of the emission peak to 445 nm. Together, these results indicate that the luminescence color of ZnO nanocrystals can be controllably adjusted through the general chemical solution methods demonstrated here. This, in turn, suggests that the oxygen-vacancy related defects that are expected to be responsible for the visible photoluminescence are sensitive to the capping ligands on the nanoparticles.

Summary of synthesis of ZnO nanostructures

Table 1 summarizes the results of this single-pot heating reaction protocol including the changes in morphology, size and photoluminescence color achieved by varying reaction conditions.

Conclusion

In summary, we have presented a general single-pot heating reaction model to controllably synthesize ZnO nanocrystals with tunable morphology, size and luminescence color. The single-pot heating method has advantages over better-established hot-injection methods, because it is less sensitive to details of mixing and therefore more amenable to scale up for large-scale production. In addition, we developed and demonstrated methods to tune the visible luminescence of ZnO nanoparticles through simple adjustment of the composition of capping ligands used in the synthesis.

References

1 C. B. Murray, D. J. Norris and M. G. Bawendi, *J. Am. Chem. Soc.*, 1993, **115**, 8706–8715.
2 A. P. Alivisatos, *Science*, 1996, **271**, 933–937.
3 A. M. Morales and C. M. Lieber, *Science*, 1998, **279**, 208–211.
4 Z. W. Pan, Z. R. Dai and Z. L. Wang, *Science*, 2001, **291**, 1947–1949.
5 M. Bruchez, M. Moronne, P. Gin, S. Weiss and A. P. Alivisatos, *Science*, 1998, **281**, 2013–2016.
6 W. C. W. Chan and S. M. Nie, *Science*, 1998, **281**, 2016–2018.
7 W. U. Huynh, J. J. Dittmer and A. P. Alivisatos, *Science*, 2002, **295**, 2425–2427.
8 I. Gur, N. A. Fromer, M. L. Geier and A. P. Alivisatos, *Science*, 2005, **310**, 462–465.
9 J. P. Clifford, K. W. Johnston, L. Levina and E. H. Sargent, *Appl. Phys. Lett.*, 2007, **91**, 253117.
10 E. H. Sargent, *Nat. Photonics*, 2009, **3**, 325–331.
11 A. McLaren, T. Valdes-Solis, G. Q. Li and S. C. Tsang, *J. Am. Chem. Soc.*, 2009, **131**, 12540–12541.
12 D. J. Gargas, M. E. Toimil-Molares and P. D. Yang, *J. Am. Chem. Soc.*, 2009, **131**, 2125–2127.
13 Y. M. Oh, K. M. Lee, K. H. Park, Y. Kim, Y. H. Ahn, J. Y. Park and S. Lee, *Nano Lett.*, 2007, **7**, 3681–3685.
14 J. V. Foreman, J. Y. Li, H. Y. Peng, S. J. Choi, H. O. Everitt and J. Liu, *Nano Lett.*, 2006, **6**, 1126–1130.
15 W. Badalawa, H. Matsui, A. Ikehata and H. Tabata, *Appl. Phys. Lett.*, 2011, **99**, 011913.
16 G. V. Naik, J. Kim and A. Boltasseva, *Opt. Mater. Express*, 2011, **1**, 1090–1099.
17 A. Boltasseva and H. A. Atwater, *Science*, 2011, **331**, 290–291.
18 M. Law, L. E. Greene, J. C. Johnson, R. Saykally and P. D. Yang, *Nat. Mater.*, 2005, **4**, 455–459.
19 A. L. Briseno, T. W. Holcombe, A. I. Boukai, E. C. Garnett, S. W. Shelton, J. J. M. Frechet and P. D. Yang, *Nano Lett.*, 2010, **10**, 334–340.
20 S. Yodyingyong, Q. F. Zhang, K. Park, C. S. Dandeneau, X. Y. Zhou, D. Triampo and G. Z. Cao, *Appl. Phys. Lett.*, 2010, **96**, 073115.
21 Z. L. Wang and J. H. Song, *Science*, 2006, **312**, 242–246.
22 X. D. Wang, J. Zhou, J. H. Song, J. Liu, N. S. Xu and Z. L. Wang, *Nano Lett.*, 2006, **6**, 2768–2772.

23 P. D. Yang, H. Q. Yan, S. Mao, R. Russo, J. Johnson, R. Saykally, N. Morris, J. Pham, R. R. He and H. J. Choi, *Adv. Funct. Mater.*, 2002, **12**, 323–331.
24 H. M. Xiong, Y. Xu, O. G. Ren and Y. Y. Xia, *J. Am. Chem. Soc.*, 2008, **130**, 7522–7523.
25 P. Zhang and W. G. Liu, *Biomaterials*, 2010, **31**, 3087–3094.
26 X. G. Peng, L. Manna, W. D. Yang, J. Wickham, E. Scher, A. Kadavanich and A. P. Alivisatos, *Nature*, 2000, **404**, 59–61.
27 R. Brayner, S. A. Dahoumane, C. Yepremian, C. Djediat, M. Meyer, A. Coute and F. Fievet, *Langmuir*, 2010, **26**, 6522–6528.
28 Y. F. Chen, M. Kim, G. Lian, M. B. Johnson and X. G. Peng, *J. Am. Chem. Soc.*, 2005, **127**, 13331–13337.
29 W. W. Yu and X. G. Peng, *Angew. Chem., Int. Ed.*, 2002, **41**, 2368–2371.
30 T. J. Boyle, S. D. Bunge, N. L. Andrews, L. E. Matzen, K. Sieg, M. A. Rodriguez and T. J. Headley, *Chem. Mater.*, 2004, **16**, 3279–3288.
31 W. W. Yu, Y. A. Wang and X. G. Peng, *Chem. Mater.*, 2003, **15**, 4300–4308.
32 M. L. Kahn, M. Monge, E. Snoeck, A. Maisonnat and B. Chaudret, *Small*, 2005, **1**, 221–224.
33 N. S. Pesika, Z. S. Hu, K. J. Stebe and P. C. Searson, *J. Phys. Chem. B*, 2002, **106**, 6985–6990.
34 S. L. Lin, N. Pradhan, Y. J. Wang and X. G. Peng, *Nano Lett.*, 2004, **4**, 2261–2264.
35 Z. H. Zhang, M. H. Lu, H. R. Xu and W. S. Chin, *Chem.–Eur. J.*, 2007, **13**, 632–638.
36 L. H. Qu, W. W. Yu and X. P. Peng, *Nano Lett.*, 2004, **4**, 465–469.
37 D. Battaglia and X. G. Peng, *Nano Lett.*, 2002, **2**, 1027–1030.
38 X. Liu, X. L. Wang, B. Zhou, W. C. Law, A. N. Cartwright and M. T. Swihart, *Adv. Funct. Mater.*, 2013, **23**, 1256–1264.
39 Y. F. Chen, E. Johnson and X. G. Peng, *J. Am. Chem. Soc.*, 2007, **129**, 10937–10947.
40 L. Manna, E. C. Scher and A. P. Alivisatos, *J. Am. Chem. Soc.*, 2000, **122**, 12700–12706.
41 M. Yang, K. Sun and N. A. Kotov, *J. Am. Chem. Soc.*, 2010, **132**, 1860–1872.
42 Y. G. Wei, Y. Ding, C. Li, S. Xu, J. H. Ryo, R. Dupuis, A. K. Sood, D. L. Polla and Z. L. Wang, *J. Phys. Chem. C*, 2008, **112**, 18935–18937.
43 L. E. Greene, B. D. Yuhas, M. Law, D. Zitoun and P. D. Yang, *Inorg. Chem.*, 2006, **45**, 7535–7543.
44 B. Liu and H. C. Zeng, *Nano Res.*, 2009, **2**, 201–209.
45 Y. Xi, J. H. Song, S. Xu, R. S. Yang, Z. Y. Gao, C. G. Hu and Z. L. Wang, *J. Mater. Chem.*, 2009, **19**, 9260–9264.
46 W. L. Hughes and Z. L. Wang, *Appl. Phys. Lett.*, 2005, **86**, 043106.
47 M. Yin, Y. Gu, I. L. Kuskovsky, T. Andelman, Y. Zhu, G. F. Neumark and S. O'Brien, *J. Am. Chem. Soc.*, 2004, **126**, 6206–6207.
48 Z. J. Gu, M. P. Paranthaman, J. Xu and Z. W. Pan, *ACS Nano*, 2009, **3**, 273–278.
49 P. X. Gao, W. J. Mai and Z. L. Wang, *Nano Lett.*, 2006, **6**, 2536–2543.
50 X. S. Tang, E. S. G. Choo, L. Li, J. Ding and J. M. Xue, *Chem. Mater.*, 2010, **22**, 3383–3388.
51 S. H. Sun, H. Zeng, D. B. Robinson, S. Raoux, P. M. Rice, S. X. Wang and G. X. Li, *J. Am. Chem. Soc.*, 2004, **126**, 273–279.
52 J. Park, E. Kang, S. U. Son, H. M. Park, M. K. Lee, J. Kim, K. W. Kim, H. J. Noh, J. H. Park, C. J. Bae, J. G. Park and T. Hyeon, *Adv. Mater.*, 2005, **17**, 429–434.
53 S. H. Sun and H. Zeng, *J. Am. Chem. Soc.*, 2002, **124**, 8204–8205.
54 S. Peng, C. Wang, J. Xie and S. H. Sun, *J. Am. Chem. Soc.*, 2006, **128**, 10676–10677.
55 V. F. Puntes, P. Gorostiza, D. M. Aruguete, N. G. Bastus and A. P. Alivisatos, *Nat. Mater.*, 2004, **3**, 263–268.
56 J. Tang and A. P. Alivisatos, *Nano Lett.*, 2006, **6**, 2701–2706.
57 W. Han, L. X. Yi, N. Zhao, A. W. Tang, M. Y. Gao and Z. Y. Tang, *J. Am. Chem. Soc.*, 2008, **130**, 13152–13161.
58 A. Singh, H. Geaney, F. Laffir and K. M. Ryan, *J. Am. Chem. Soc.*, 2012, **134**, 2910–2913.

